Hindawi
Advances in Civil Engineering
Volume 2018, Article ID 2972931, 11 pages
https://doi.org/10.1155/2018/2972931

Research Article

Experimental and Numerical Analysis of Nonlinear Flexural Behaviour of Lattice-Web Reinforced Foam Core Composite Sandwich Panels

Jiye Chen,[1] Hai Fang,[1] Weiqing Liu,[2] Yujun Qi,[1] and Lu Zhu[1]

[1]*College of Civil Engineering, Nanjing Tech University, Nanjing 211816, China*
[2]*Advanced Engineering Composites Research Center, Nanjing Tech University, Nanjing 211816, China*

Correspondence should be addressed to Hai Fang; fanghainjut@163.com

Received 10 August 2018; Revised 21 October 2018; Accepted 7 November 2018; Published 21 November 2018

Academic Editor: Flavio Stochino

This paper conducted experimental and numerical analysis of the nonlinear flexural behaviour of lattice-web reinforced foam core composite sandwich panels. Composite sandwich panels composed of a polyurethane (PU) foam core with glass fibre-reinforced polymer (GFRP) composites as the face sheets and lattice webs were fabricated through the vacuum infusion moulding process (VIMP). The flexural behaviour of these composite sandwich panels were experimentally investigated under both uniformly distributed and concentrated loading scenarios. The results showed that reinforced lattice webs can significantly increase the flexural stiffness and load-carrying capacity of sandwich panels and effectively postpone the onset of interfacial debonding failure between the face sheets and core. The effects of the lattice-web height and spacing on the ductility and load-carrying capacities of the sandwich panels were also analysed. Several numerical simulations on lattice-web reinforced foam core composite sandwich panels under concentrated loadings were also conducted. The effectiveness of the finite element (FE) model was validated by the experimental work. Parametric studies indicated that thicker face sheets and lattice webs can remarkably increase the load-carrying capacity. Moreover, the load-carrying capacity and midspan deflection were hardly affected by the foam density.

1. Introduction

Composite sandwich structures have been widely employed in aviation, military, transport, and civil applications as a result of their unique characteristics, including their high strength, high stiffness-to-weight ratio, structural designability, and excellent corrosion resistance [1–3]. Low-density materials such as foam, honeycomb cells, and balsa wood are usually adopted as the core of composite sandwich structures, thereby contributing to a high stiffness along the face sheets to resist loadings. The face sheets are generally made of various fibre (e.g., glass, aramid, or carbon) reinforced polymer composites. From a structural perspective, the face sheets provide a major contribution to the bending stiffness, while the core provides a major component of the shear stiffness of a sandwich structure [1].

A large number of experimental and analytical studies on sandwich structures with different types of cores have been carried out over the past three decades [4–9]. Sharaf et al. [10] studied the uniaxial bending behaviour of ten foam-filled sandwich panels experimentally. The test results demonstrated that the bending strength and stiffness of sandwich panels increased significantly with an increase in the foam density; meanwhile, a considerable horizontal slip occurred between the top face sheet and the core due to the low toughness of the foam core. Prakash et al. [11] investigated the maximum impact load, energy absorption, and failure modes of honeycomb sandwich panels with various cells through low-velocity impact tests. Their test results showed that the core buckled at relatively low energy levels but crushed at higher levels. Steeves and Fleck [12, 13] conducted experimental and analytical investigations on the collapse mechanisms of simply supported sandwich beams composed of glass fibre-reinforced polymer (GFRP) face sheets and a polyvinyl chloride (PVC) foam core that were loaded under three-point bending. The experimental results

demonstrated that the failure mode was dependent on the beam geometry and the density of the foam core. Moreover, they found that the ultimate bending strength and initial stiffness of the sandwich panels were relatively small because no lattice web or fibre insertions were utilized to improve the core stiffness. Keller et al. [14] manufactured a low-storey building in Lausanne, Switzerland, using pultruded GFRP profiles as structural members, e.g., beam and columns, and GFRP/foam sandwich panels as the roof structure. Manalo et al. [15] fabricated GFRP sandwich beams by using an adhesive to bond the GFRP skins to the phenolic foam cores. Interfacial debonding was found to be the main failure mode when such beams were subjected to flexural loading. Based on the above mentioned studies, it seems that the weakness of the interfacial debonding between the face sheets and the core within a traditional sandwich structure reduces its load-carrying capacity and therefore limits its structural application.

A lattice-web reinforced composite sandwich structure was proposed to overcome this weakness; the insertion of GFRP into the lattice web prevents debonding between the face sheets and core and enhances the compressive strength of the sandwich structure [16–19]. James et al. [20] investigated the flexural performance of one-way lattice-web reinforced GFRP composite sandwich structures; the typical failure modes included core shear failure, local indentation, and debonding or delamination between the core and face sheets. To achieve a better mechanical performance than those of one-way lattice-web reinforced structures, two-way lattice-web reinforced composite sandwich structures with lattice-web reinforcements in both the longitudinal direction and the transverse direction were fabricated through the vacuum infusion moulding process (VIMP) technique and studied. Such lattice-web reinforced sandwich panels [21, 22] showed a significant increase in the load-carrying capacity under compression and bending due to the improved resistance to interfacial debonding between the face sheets and the core. Moreover, this kind of composite sandwich panel has been applied in some construction projects, as shown in Figure 1. Figure 1(a) shows a footbridge using two-way lattice-web reinforced foam core composite sandwich panels as bridge decks, which can sustain a crowd. Figure 1(b) shows a temporary house using two-way lattice-web reinforced foam core composite sandwich panels as roof panels and wall panels. Nevertheless, to understand the mechanical behaviour of the components of sandwich panels, the bending behaviour of such panels must be investigated.

The present study investigated the flexural behaviour of two-way lattice-web reinforced foam core composite sandwich panels under both uniformly distributed and concentrated loading through experimental and numerical studies. Uniformly distributed and concentrated loading tests were carried out on square composite sandwich panels with four simply supported edges as the boundary conditions. The load-deflection relationships and failure modes of the sandwich panels with different lattice-web geometries were reported. Numerical simulations using finite element (FE) modelling were also carried out and compared with the experimental results. Furthermore, parametric studies on the effects of the face-sheet thickness, lattice-web thickness, and foam density were analysed and discussed in this paper.

(a)

(b)

Figure 1: Practical constructions using two-way lattice-web reinforced foam core composite sandwich panels as the main loading-bearing components: (a) a footbridge using sandwich panels as bridge decks and (b) a temporary house using sandwich panels as roof panels and wall panels.

2. Experimental Program

2.1. Test Specimens and Material Properties. The proposed lattice-web reinforced foam core composite sandwich panels are illustrated in Figure 2, in which the core is composed of small sliced foam blocks wrapped with glass fibre fabrics as reinforcing webs in both the longitudinal and the transverse directions. These composite sandwich panels were manufactured through the VIMP process. Different series of specimens were prepared to investigate the performance of the composite sandwich panels, as listed in Table 1, where the label OS represents sandwich panels without lattice web, and the label TS represents sandwich panels reinforced with lattice webs. Specimens with different core heights (50 mm, 75 mm, and 100 mm) and lattice-web spacing values (75 mm, 125 mm, and 175 mm) and the same face-sheet thickness (1.6 mm) were prepared as described in Table 1.

The material properties were determined through coupon tests. For the GFRP face sheets composed of unsaturated polyester resin and biaxial [0°/90°] glass fibre fabrics, the

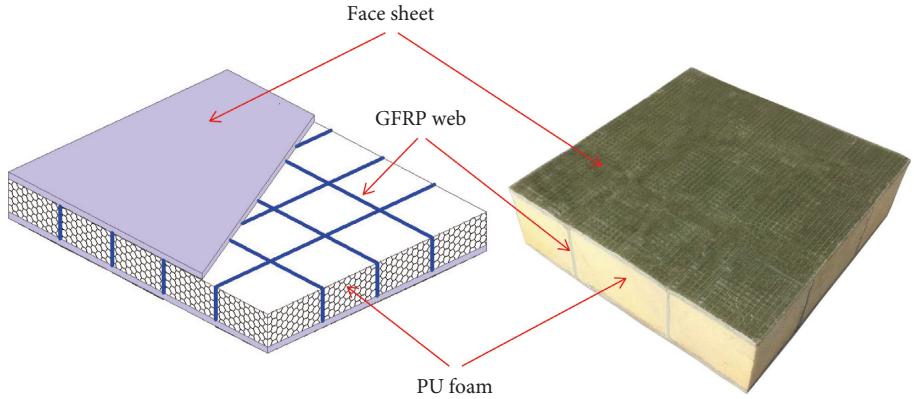

Figure 2: Foam core sandwich panels with lattice-web reinforcements.

Table 1: Description of the specimens.

Specimen	L_x (mm) Specimen length	L_y (mm) Specimen width	s (mm) Lattice spacing	h (mm) Core height	H (mm) Specimen total height	t_w (mm) Lattice-web thickness	t_s (mm) Face-sheet thickness
OS50	1000	1000	—	50	53.2	1.6	1.6
OS75	1000	1000	—	75	78.2	1.6	1.6
OS100	1000	1000	—	100	103.2	1.6	1.6
TS75-50	1000	1000	75	50	53.2	1.6	1.6
TS75-75	1000	1000	75	75	78.2	1.6	1.6
TS75-100	1000	1000	75	100	103.2	1.6	1.6
TS125-75	1000	1000	125	75	78.2	1.6	1.6
TS175-75	1000	1000	175	75	78.2	1.6	1.6

[1]OS represents ordinary sandwich panels (PU core) without lattice-web reinforcements, and the following number (e.g., 50, 75, and 100) represents the height of the core. [2]TS represents lattice-web reinforced sandwich panels; the first number (e.g., 75, 125, and 175) represents the spacing between the lattice webs, and the following number (e.g., 50, 75, and 100) represents the web height.

tensile strength and elastic modulus are 322.9 MPa and 20.95 GPa, respectively, according to standard ASTM D3039 [23]. For the GFRP lattice web composed of unsaturated polyester resin and biaxial [−45°/45°] glass fibre fabrics, the tensile strength and elastic modulus are 296.3 MPa and 6.41 GPa, respectively, and the shear modulus is 5.82 GPa according to standard ASTM D2344 [24]. Polyurethane (PU) foam with a density of 60 kg/m^3 was used to form the core. The stress-strain curve of the PU foam is shown in Figure 3; according to standard ASTM D1621 [25], the initial elastic modulus and the compressive strength of the PU foam are 7.17 MPa and 0.28 MPa, respectively, whereas the shear modulus and strength (ASTM C273 [26]) are 2.08 MPa and 0.29 MPa, respectively, and Poisson's ratio is 0.3.

2.2. Experimental Setup. The lattice-web reinforced foam core sandwich panels were simply supported on a 1 m × 1 m square steel frame that was composed of four I-section steel beams welded together. The sandwich panels were tested under two loading scenarios: (1) uniformly distributed loading (UDL), which was applied by the gravity of accumulated balance weights, as shown in Figure 4 and (2) concentrated loading, which was applied to the centre of the face sheet by a hydraulic jack at a rate of 2 mm per min, as shown in Figure 5.

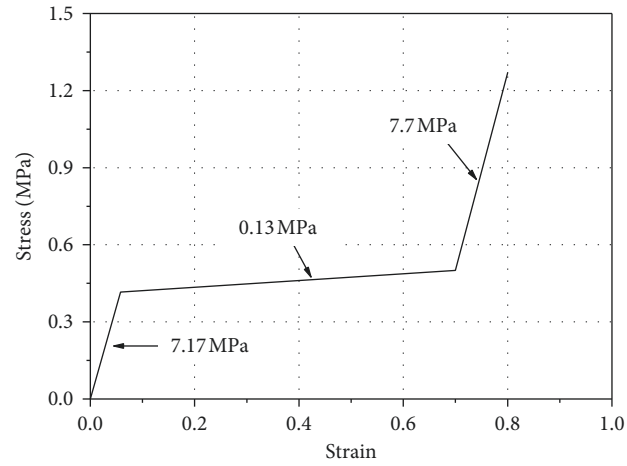

Figure 3: The trilinear equivalent stress-strain curve of the PU foam core.

3. Experimental Results and Discussion

3.1. Uniformly Distributed Loading (UDL). The aim of a UDL test is to evaluate the flexural stiffness of a specimen; thus, specimens are loaded within the elastic region, and they do not reach ultimate failure. Figure 6(a) presents the load-midspan deflection curves of the lattice-web reinforced foam core sandwich panels with different web heights; the bending

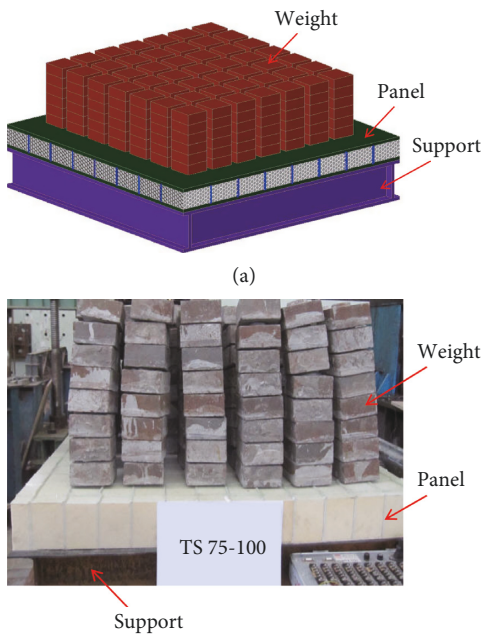

Figure 4: UDL test setup: (a) schematic diagram and (b) photograph.

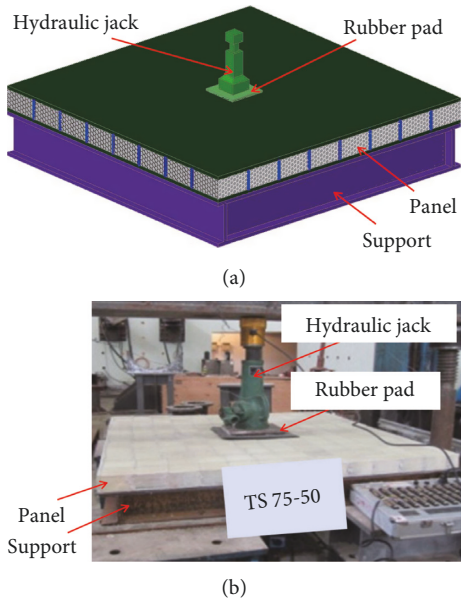

Figure 5: Concentrated loading test setup: (a) schematic diagram and (b) photograph.

stiffness is calculated according to the slope of the load-deflection curve. The stiffnesses of the sandwich panels with web heights of 75 mm (specimen TS75-75) and 100 mm (specimen TS75-100) increased by 100% and 88.8%, respectively, relative to specimen TS75-50 with a web height of 50 mm. Therefore, an increment in the web height can significantly increase the flexural stiffness of sandwich panels. Similarly, the influence of the lattice spacing on the flexural stiffness of sandwich panels with the same web height is presented in Figure 6(b), which demonstrates that increments in the web spacing from an initial value of 75 mm to 125 mm and 175 mm caused the flexural stiffness to decrease by 12.1% and 18.2%, respectively. Therefore, an increment in the web spacing can decrease the flexural stiffness of composite sandwich panels; however, the magnitude of the stiffness reduction is small.

3.2. Concentrated Loading

3.2.1. Failure Modes. Concentrated loading tests were performed on the composite sandwich panels with four simply supported edges until they reached ultimate failure. The effects of the reinforcement, height, and spacing of the lattice web on the failure modes and load-carrying capacities were investigated.

(1) Effect of the Lattice-Web Height. For specimens TS75-50, TS75-75, and TS75-100, all of which have the same web spacing (75 mm) but different web heights (50 mm, 75 mm, and 100 mm), the failure modes were similar. For specimen TS75-50, local debonding between the top face sheet and the core was first observed when the applied load reached 36.2 kN, and several perpendicular cracks initiated alongside the loading jack. When the applied load reached 53.2 kN, a loud noise was heard, and the top face sheet exhibited buckling failure, while the glass fibres failed by cracking. The corresponding maximum midspan deflection was 40.5 mm. Specimens TS75-75 and TS75-100 followed similar failure processes, and the corresponding ultimate loads at failure were 83.3 kN and 108.8 kN, respectively. Figure 7 shows the failure mode on TS75-75 at the ultimate load. The maximum midspan deflections for TS75-75 and TS75-100 were 27.6 mm and 25.7 mm, respectively.

(2) Effect of the Lattice-Web Spacing. Interfacial debonding between the top face sheet and core was the dominant failure mode for specimens TS75-75, TS125-75, and TS175-75, all of which have the same lattice-web height (75 mm) but different lattice-web spacing values (75 mm, 125 mm, and 175 mm). However, the interfacial debonding observed in specimen TS175-75 was more severe than that observed in specimens TS75-75 and TS125-75. During the loading, slight local debonding was initially observed in specimen TS175-75 between the top face sheet and core along with several cracks when the load reached 38.2 kN. This local debonding that initiated on the top face sheet gradually propagated to the four edges of the sandwich panel with an increasing load, leading to interfacial debonding failure between the top face sheet and the core, as shown in Figure 8. The ultimate loads for specimens TS125-75 and TS175-75 were 65 kN and 49.8 kN, respectively, and the corresponding maximum midspan deflections were 29.1 mm and 31.2 mm.

(3) Effect of the Lattice-Web Reinforcement. For specimen OS50, which does not have a reinforced lattice web, a slight splitting sound was heard that originated from the top face sheet at an applied load of 11.5 kN. When the load reached 27.2 kN, an abrupt and loud sound was heard coincident

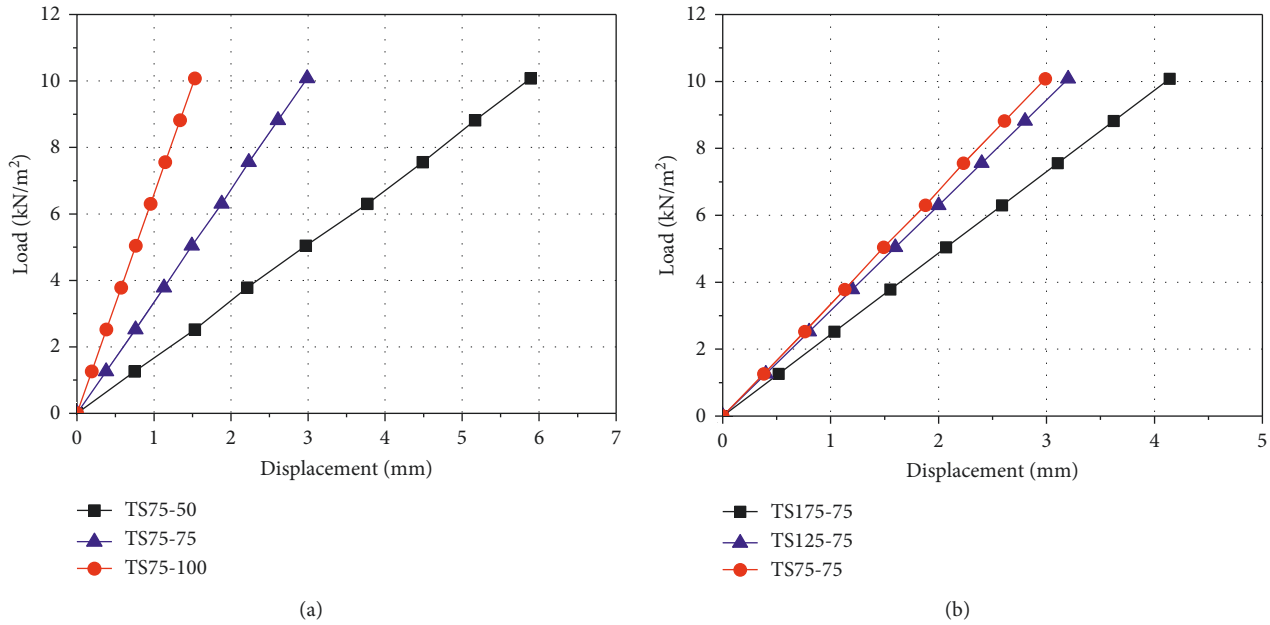

Figure 6: Load-midspan deflection curves of specimens (a) with different web heights and (b) with different web spacing values.

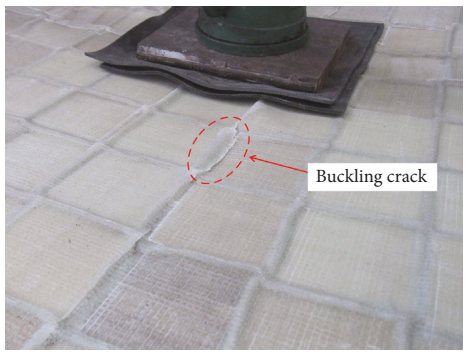

Figure 7: Failure mode of specimen TS75-75.

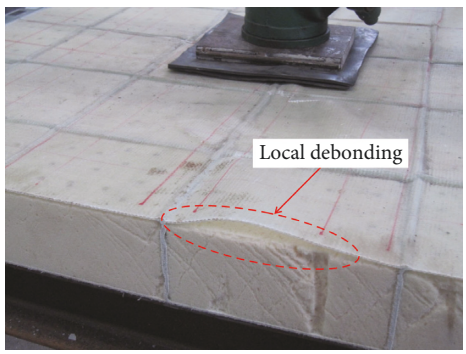

Figure 8: Failure mode of specimen TS175-75.

with a sharp drop in the applied load, indicating that the specimen experienced brittle failure due to the clear splitting sound originating from the surface of the top face sheet. This brittle failure is attributed to the large-scale debonding between the top face sheet and the core. The failure modes of specimens OS75 and OS100 were similar to that of specimen OS50. The ultimate loads of specimens OS50, OS75, and OS100 were 27.2 kN, 29.3 kN, and 32 kN, respectively, and the corresponding maximum midspan deflections were 32.1 mm, 26.5 mm, and 20.5 mm.

3.2.2. Load-Displacement Curves. The load-midspan deflection curves are shown in Figure 9, and the results are analysed below.

(1) Comparing the results of specimens TS75-50, TS75-75, and TS75-100, all of which have the same lattice-web spacing values, reveals that an increase in the web height substantially increases the flexural stiffness and load-carrying capacity of sandwich panels, but the magnitude of this effect decreases as the web height increases. As shown in Figure 9(a), with an increment in the web height from the original value of 50 mm to 75 mm and 100 mm, the load-carrying capacities increased by 56.6% and 30.6%, respectively, and the corresponding maximum midspan deflections decreased by 31.8% and 6.9%.

(2) Comparing the results of specimens TS75-75, TS125-75, and TS175-75, all of which have the same lattice-web height, demonstrates that a decrease in the web spacing effectively increases the flexural stiffness and load-carrying capacity of sandwich panels and reduces the maximum midspan deflection; however, the effect is not evident. As shown in Figure 9(b), decreases in the web spacing from the original value of 175 mm to 125 mm and 75 mm caused the load-carrying capacities to increase by 30.5% and 28.2%, respectively, and the corresponding maximum midspan deflections decreased by 6.7% and 5.2%.

(3) In contrast to the load-carrying capacity of sandwich panels without lattice-web reinforcements, the load-carrying capacity of lattice-web reinforced sandwich

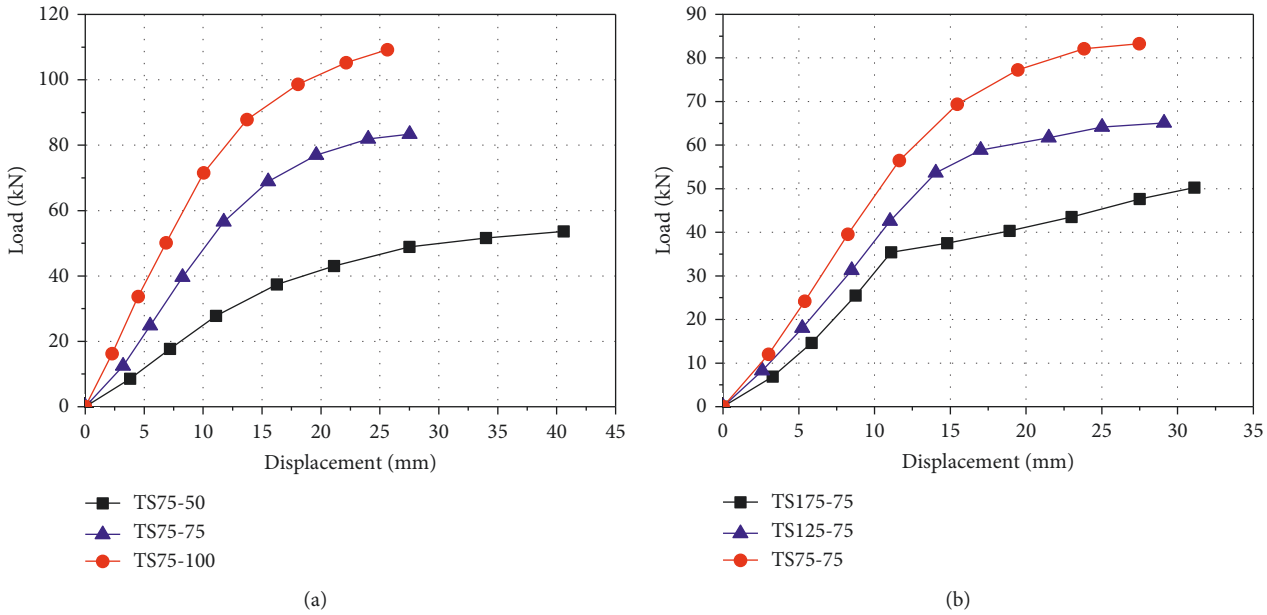

Figure 9: Load-midspan deflection curves of specimens (a) with different web heights and (b) with different web spacing values.

panels increased significantly, i.e., the ultimate loads of lattice-web sandwich panel specimens TS75-75 and TS125-75 were 83.3 kN and 65.0 kN, but sandwich panel specimen OS75 without lattice-web reinforcements had an ultimate load of only 18.3 kN. The unreinforced sandwich panel specimen experienced brittle failure, and the large-scale interfacial debonding between the top face sheet and the core constituted the final failure mode. In contrast, ductile failure was observed during the flexural testing of the lattice-web reinforced sandwich panels.

(4) Although composite face sheets and shear cores are brittle materials, the sandwich panel specimens exhibited ductility after implementing lattice-web reinforcements between the two types of materials; therefore, the nonlinearity was sustained during the failure process. Such ductility can be called "pseudoductility" [14] because it is not caused by the materials themselves but by the gradual debonding along the interfaces between the GFRP members and core materials. The ductility coefficient μ, which is expressed as Formula (1), can be used to examine such pseudoductility [27].

$$\mu = \frac{D_u}{D_y}, \tag{1}$$

where D_u is the maximum displacement of a structural member under the ultimate load and D_y is the maximum displacement of the structural member under the elastic yielding load.

The elastic yielding point can be determined using the method from [28], i.e., the yielding point is the point on the curve with a tangent slope that is identical to the slope of the straight line connecting the origin point to the peak point; if there are two or more points, the yielding point can be determined from the projection of the average load values. The load capacity and displacement at the elastic limit, the ultimate load capacity, the ultimate displacement, and the ductility coefficient are listed in Table 2. The testing results obtained from specimens TS75-75, TS125-75, and TS175-75 (with the same core height of 75 mm) showed that their ductility coefficients increased with an increase in the web spacing. However, for the specimen with no lattice web, which corresponds to an infinite web spacing, the ductility coefficient was a minimum (equal to 1). Hence, this analysis is effective only when the web spacing exceeds a certain value. The initial ductility coefficient of specimen TS75-75 is 1.7; the ductility coefficients corresponding to increases in the web spacing from 75 mm to 125 mm and 175 mm were 2.0 and 2.6, e.g., the ductility coefficient increased by 17.6% and 30.0%. This pseudoductility is attributed to the interfacial debonding between the core materials and face sheets, as shown in Figure 8 for specimen TS175-75. Specimens TS75-50, TS75-75, and TS75-100 (with the same web spacing of 75 mm) showed similar ductility coefficients, e.g., 2.0, 1.7, and 1.9, respectively, with increases in the web height from 50 mm to 75 mm and 100 mm. The three specimens showed similar failure modes, e.g., buckling failure on the top face sheet, as shown in Figure 7 for specimen TS75-75.

4. Finite Element Analysis

4.1. Finite Element Modelling. ANSYS/LS-DYNA software is utilized to simulate the load-displacement responses of the lattice-web reinforced foam core composite sandwich panels subjected to concentrated loading. As shown in Figure 10, in this model, a movable rigid loading cell is placed on the top of the sandwich panel. The nodes

Table 2: Experimental results of the ultimate load capacity, displacement, and ductility coefficient.

Specimen	Bearing capacity at elastic limit (kN)	Displacement at elastic limit D_y (mm)	Ultimate bearing capacity (kN)	Ultimate displacement D_u (mm)	Ductility coefficient μ
OS50	27.2	32.1	27.2	32.1	1
OS75	18.3	16.5	18.3	16.5	1
OS100	32.0	20.5	32.0	20.5	1
TS75-50	39.9	19.8	53.2	40.5	2.0
TS75-75	71.3	16.2	83.3	27.6	1.7
TS75-100	87.5	13.6	108.8	25.7	1.9
TS125-75	52.6	14.3	65.0	29.1	2.0
TS175-75	35.6	12.1	49.8	31.2	2.6

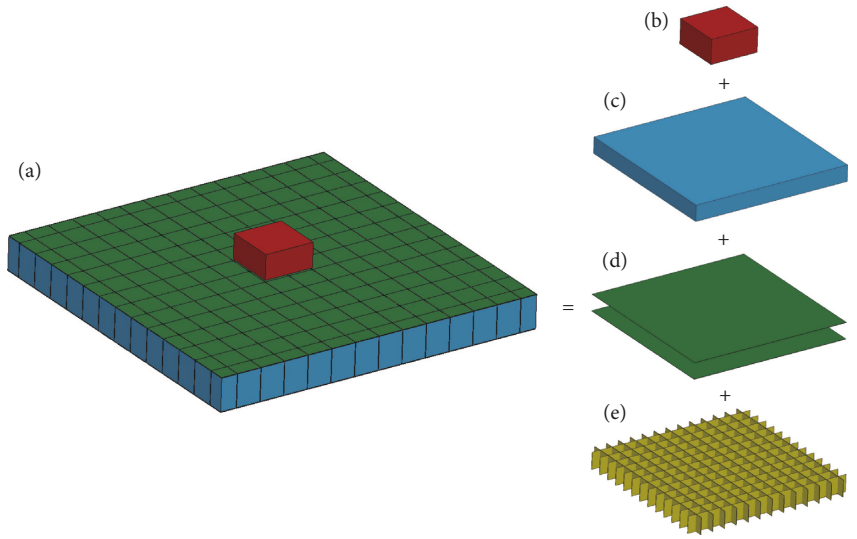

Figure 10: Model geometry: (a) specimen TS75-100; (b) rigid loading cell; (c) PU foam core; (d) face sheets; (e) lattice webs.

along the interface are merged assuming that sliding does not occur between the composite materials and the foam core.

4.1.1. Element Type. The GFRP face sheets and lattice webs were simulated with Belytschko-Tsay shell elements [29]. The shell element is widely used during research on thin-walled structures because of its remarkable efficiency arising from adopting a reduced integration technique. The rigid loading cell and PU foam core were modelled using solid elements, which were also formulated with the reduced integration method. The mesh size was successively refined until an optimum result was achieved.

4.1.2. Material Model. The GFRP face sheets and lattice webs were modelled using an available material model MAT 54 (enhanced composite damage), which was utilized with optional brittle failure formulated by Chang [30, 31]. The Chang-Chang failure criterion is given as Formulas (2)–(5). ∗PART_COMPOSITE was used to define the thickness and material angle for each composite layer. Tables 3 and 4 list the mechanical properties of the GFRP face sheets and lattice webs, respectively, obtained from the experiments. The PU foam was modelled using MAT 63 (crushable foam), which is expert at modelling crushable foam with optional tension cutoff and damping. In this work, the tensile stress cutoff and damping coefficient were set to 1 MPa and 0.5, respectively. Figure 3 shows the trilinear equivalent stress-strain curve of the PU foam. The data points of the curve were used to put into the simulation. In addition, a failure criterion was used for MAT 63, and once the maximum principal strain reaches 0.1, the element is deleted from the calculation [32].

For the tensile fibre mode, where $\sigma_{aa} > 0$:

$$e_f^2 = \left(\frac{\sigma_{aa}}{X_t}\right)^2 + \beta\left(\frac{\sigma_{ab}}{S_c}\right)^2 - 1 \quad \begin{cases} \geq 0 \text{ failed,} \\ < 0 \text{ elastic,} \end{cases} \tag{2}$$

where $E_a = E_b = G_{ab} = \nu_{ab} = \nu_{ba} = 0$ upon failure, β is a weighting factor for the shear term with a range of 0-1, σ_{aa} is the stress in the fibre direction, σ_{ab} is the transverse shear stress, X_t is the tensile strength in the fibre direction, and S_c is the shear strength. In this work, the weighting factor β is set to 0.5.

For the compressive fibre mode, where $\sigma_{aa} < 0$:

$$e_c^2 = \left(\frac{\sigma_{aa}}{X_c}\right)^2 - 1 \quad \begin{cases} \geq 0 \text{ failed,} \\ < 0 \text{ elastic,} \end{cases} \tag{3}$$

where $E_a = \nu_{ab} = \nu_{ba} = 0$ upon failure and X_c is the compressive strength in the fibre direction.

Table 3: Material parameters of the GFRP face sheets.

Property	LS-DYNA parameter	Experimental value
Density	RO	1.8 g/cm^3
Modulus in longitudinal direction	EA	20.95 GPa
Modulus in transverse direction	EB	20.95 GPa
Shear modulus	GAB	2.5 GPa
Poisson's ratio	PRBA	0.15
Tensile strength in longitudinal direction	XT	322.9 MPa
Tensile strength in transverse direction	YT	322.9 MPa
Compressive strength in longitudinal direction	XC	165.4 MPa
Compressive strength in transverse direction	YC	165.4 MPa
Shear strength	SC	55 MPa

Table 4: Material parameters of GFRP lattice webs.

Property	LS-DYNA parameter	Experimental value
Density	RO	1.8 g/cm^3
Modulus in longitudinal direction	EA	6.41 GPa
Modulus in transverse direction	EB	6.41 GPa
Shear modulus	GAB	5.82 GPa
Poisson's ratio	PRBA	0.15
Tensile strength in longitudinal direction	XT	296.3 MPa
Tensile strength in transverse direction	YT	296.3 MPa
Compressive strength in longitudinal direction	XC	149.8 MPa
Compressive strength in transverse direction	YC	149.8 MPa
Shear strength	SC	75 MPa

For the tensile matrix mode, where $\sigma_{bb} > 0$:

$$e_m^2 = \left(\frac{\sigma_{bb}}{Y_t}\right)^2 + \left(\frac{\sigma_{ab}}{S_c}\right)^2 - 1 \quad \begin{cases} \geq 0 \text{ failed}, \\ < 0 \text{ elastic}, \end{cases} \tag{4}$$

where $E_b = \nu_{ba} = G_{ab} = 0$ upon failure, σ_{bb} is the stress normal to the fibre direction, Y_t is the tensile strength normal to the fibre direction, and Y_c is the compressive strength normal to the fibre direction.

For the compressive matrix mode, where $\sigma_{bb} < 0$:

$$e_d^2 = \left(\frac{\sigma_{bb}}{2S_c}\right)^2 + \left[\left(\frac{Y_c}{2S_c}\right)^2 - 1\right]\frac{\sigma_{bb}}{Y_c} + \left(\frac{\sigma_{ab}}{S_c}\right)^2 - 1 \quad \begin{cases} \geq 0 \text{ failed}, \\ < 0 \text{ elastic}, \end{cases} \tag{5}$$

where $E_b = \nu_{ba} = \nu_{ab} = G_{ab} = 0$ upon failure.

4.1.3. Loading and Contact Conditions. The concentrated loading was achieved by moving the rigid loading cell with a constant velocity. The vertical displacements of the nodes on all four sides of the bottom of the panel were constrained. The rigid loading cell was constrained in all degrees of freedom apart from the vertical displacement. A rate of 2 mm/min was applied to the loading cell in the direction of the vertical displacement. In order to model the interaction between the rigid loading cell and the specimen, an "automatic surface to surface" contact was defined following the suggestion of Yin [33] and Zhang [34].

4.1.4. Concentrated Loading Simulation. To obtain numerical stability in an explicit simulation, the time step is usually small. However, a small time step is not suitable for concentrated loading simulation because an enormous amount of steps are required for the concentrated loading simulation. Two approaches have been commonly used to minimize the computational time: (1) scaling up the loading cell velocity and/or (2) scaling up the mass density [35]. In this work, the real rate of 2 mm/min is replaced by 50 mm/s. Such an approach attains a concentrated loading process, for the ratio of the kinetic energy to the internal energy is less than 1.5% during the loading process, as shown in Figure 11.

4.2. Validation of the Finite Element Model. Validation of the FE model is one of the most important steps in the model building process. The FE model for concentrated loading is validated by comparing the load-displacement curve with the experimental results.

Figure 12 shows a comparison of the load-displacement curves between the experimental results and numerical simulations. During the initial loading step, the load-displacement curve behaves linearly with a high slope, and the slope gradually decreases with an increase in the load until reaching ultimate failure. The ultimate load from the FE analysis is 116.5 kN, which is 7.5% higher than the experimental result of 108.4 kN, and the ultimate displacement from the FE analysis is 23.3 mm, which is 9.3% less than the experimental result of 25.7 mm. The numerical simulation accurately predicts the crushing behaviour, although there is a small difference between the experimental results and the predicted loads. Considering the complexity of the model, this comparison shows that the proposed FE model can greatly predict the responses of the test specimens.

5. Parametric Studies

The previous section proved the reliability of the FE modelling approach; therefore, additional parametric studies were carried out on the effects of the face-sheet thickness, lattice-web thickness, and foam density on the flexural performance of the composite sandwich panels using FE modelling, the results of which are discussed in this section.

5.1. Effect of the Face-Sheet Thickness. Figure 13 shows the effect of the face-sheet thickness on the load-carrying capacity and midspan deflection under the same lattice-web height (h = 100 mm), lattice-web spacing (s = 75 mm), lattice-web thickness (t_w = 1.6 mm), and foam density (ρ = 60 kg/m^3). When the face-sheet thicknesses were 1.6 mm, 2.4 mm, 3.2 mm, and 4.0 mm, the load-carrying capacities

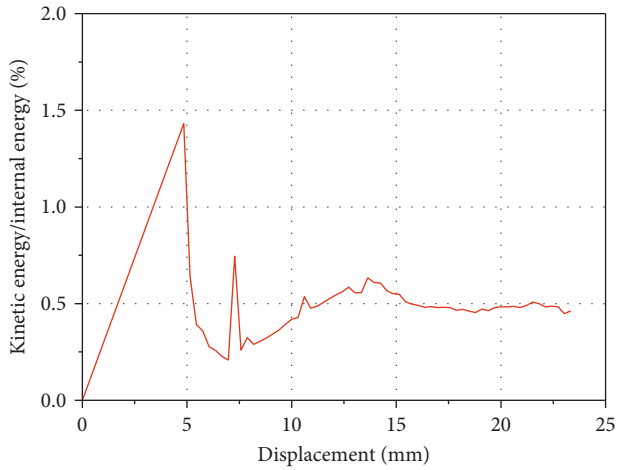

Figure 11: Ratio of the kinetic energy to the internal energy of specimen TS75-100.

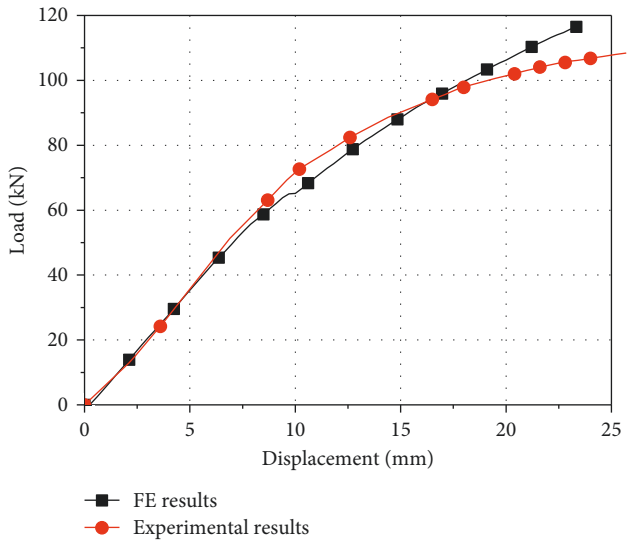

Figure 12: Comparison of the experimental and numerical load-displacement curves of specimen TS75-100.

were 116.5 kN, 153.4 kN, 180.8 kN, and 197.4 kN, respectively, and the corresponding midspan deflections were 23.3 mm, 21.3 mm, 19.7 mm, and 17.3 mm. Hence, the use of thicker face sheets can achieve a significantly larger load-carrying capacity but a smaller midspan deflection.

5.2. Effect of the Lattice-Web Thickness. Figure 14 shows the effect of the lattice-web thickness on the load-carrying capacity and midspan deflection under the same lattice-web height (h =100 mm), lattice-web spacing (s = 75 mm), face-sheet thickness (t_w = 1.6 mm), and foam density (ρ = 60 kg/m^3). When the lattice-web thicknesses were 1.6 mm, 2.4 mm, 3.2 mm, and 4.0 mm, the load-carrying capacities were 116.5 kN, 134.0 kN, 142.8 kN, and 150.9 kN, respectively, and the corresponding midspan deflections were 23.3 mm, 22.7 mm, 22.3 mm, and 22.0 mm. Therefore, increasing the lattice-web thickness can result in a larger load-carrying

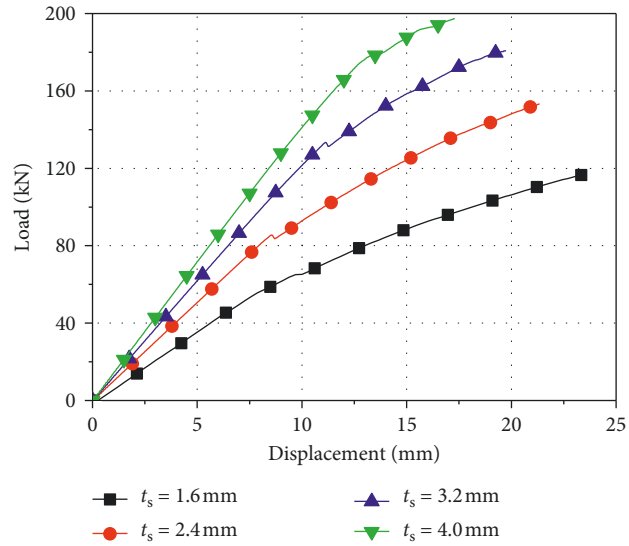

Figure 13: Effect of the face-sheet thickness (h = 100 mm, s = 75 mm, t_w = 1.6 mm, and ρ = 60 kg/m^3).

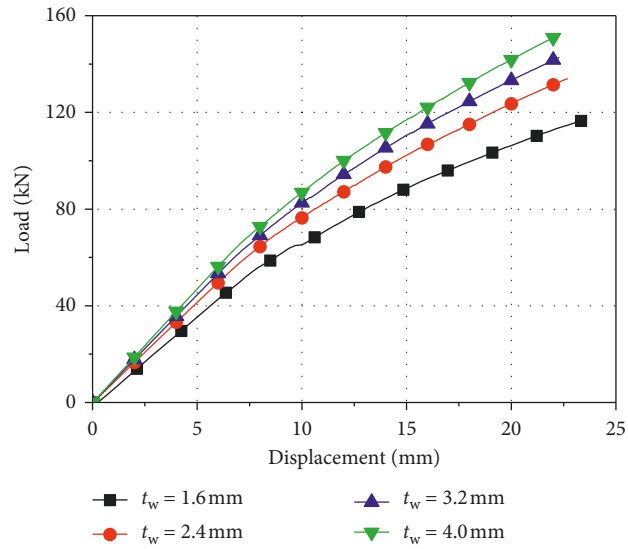

Figure 14: Effect of the lattice-web thickness (h = 100 mm, s = 75 mm, t_s = 1.6 mm, and ρ = 60 kg/m^3).

capacity. However, the differences in the midspan deflections among these four panels were negligible.

5.3. Effect of the Foam Density. Figure 15 shows the effect of the foam density on the load-carrying capacity and midspan deflection under the same lattice-web height (h = 100 mm), lattice-web spacing (s = 75 mm), face-sheet thickness (t_s = 1.6 mm), and lattice-web thickness (t_w = 1.6 mm). The stress-strain data points of the PU foam with different foam densities are listed in Table 5 [32]. When the foam densities were 40 kg/m^3, 60 kg/m^3, 80 kg/m^3, and 100 kg/m^3, the load-carrying capacities were 115.0 kN, 116.5 kN, 119.1 kN, and 119.6 kN, respectively, and the corresponding midspan deflections were 23.5 mm, 23.3 mm, 23.1 mm, and 23.0 mm.

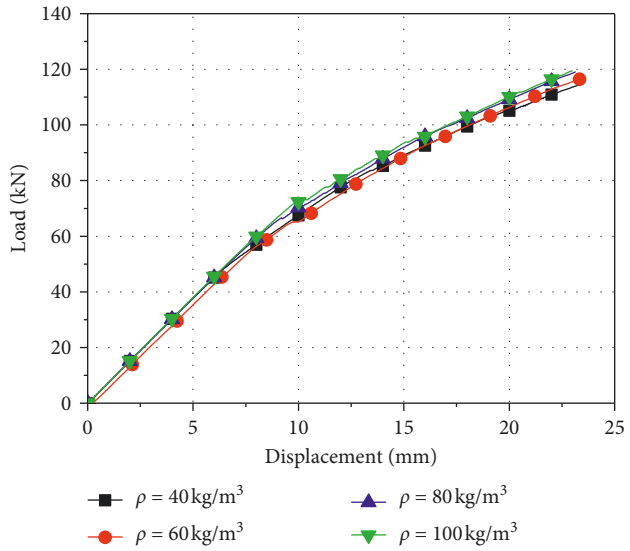

Figure 15: Effect of the foam density (h = 100 mm, s = 75 mm, t_s = 1.6 mm, and t_w = 1.6 mm).

Table 5: Stress-strain data points of PU foam with different densities [32].

Density (kg/m^3)					
40	σ_{True} (MPa)	0	0.151	0.4	1.25
	ε	0	0.05	0.8	0.83
60	σ_{True} (MPa)	0	0.416	0.5	1.27
	ε	0	0.058	0.7	0.8
80	σ_{True} (MPa)	0	0.504	0.87	1.81
	ε	0	0.049	0.67	0.78
100	σ_{True} (MPa)	0	0.703	1.39	2.69
	ε	0	0.045	0.63	0.76

The differences in the load-carrying capacities and midspan deflections among these four panels were negligible. Hence, the load-carrying capacity and midspan deflection were hardly affected by the foam density.

6. Conclusions

This paper investigated the nonlinear flexural behaviours of foam core composite sandwich panels with and without lattice-web reinforcements through UDL and concentrated loading tests. The effects of various geometric parameters on the flexural performance of the sandwich panels were analysed and discussed through nonlinear experimental and numerical modelling. The following conclusions can be drawn from this work:

(1) The failure mode of ordinary composite sandwich panels without lattice-web reinforcements under compression is interfacial debonding between the core and face sheets. However, the onset of interfacial debonding failure can be delayed for sandwich panels with two-way lattice-web reinforcements. The introduction of lattice webs can improve the composite action between the core and the face sheets and substantially increase both the flexural stiffness and the ultimate load capacity of composite sandwich panels.

(2) The main failure mode for composite sandwich panels with lattice-web reinforcements is buckling failure together with the breakage of glass fibres on the face sheets. The failure modes are similar for sandwich panel specimens with different web heights; however, local interfacial debonding occurred between the core and the face sheets, and this local interfacial debonding failure mode became more evident as the lattice web spacing increased.

(3) An FE model was developed, and simulations of the concentrated loading showed good agreement with the experimental results. Parametric studies based on the verified model demonstrated that thicker face sheets and lattice webs can remarkably increase the load-carrying capacity. However, the load-carrying capacity and midspan deflection were hardly affected by the foam density.

Data Availability

The data used to support the findings of this study are available from the corresponding author upon request.

Conflicts of Interest

The authors declare that there are no conflicts of interest regarding the publication of this paper.

Acknowledgments

This research was supported by the National Natural Science Foundation of China (Grant nos. 51578285 and 51778285) and the Natural Science Foundation of Jiangsu Province (Grant no. BK20161545).

References

[1] H. G. Allen, *Analysis and Design of Structural Sandwich Panels*, Pergamon Press, London, UK, 1969.

[2] H. Fang, H. Y. Shi, Y. Wang, Y. J. Qi, and W. Q. Liu, "Experimental and theoretical study of sandwich panels with steel facesheets and GFRP core," *Advances in Materials Science and Engineering*, vol. 2016, Article ID 7159205, 12 pages, 2016.

[3] H. Fang, Y. F. Mao, W. Q. Liu, L. Zhu, and B. Zhang, "Manufacturing and evaluation of large-scale composite bumper system for bridge pier protection against ship collision," *Composite Structures*, vol. 158, pp. 187–198, 2016.

[4] J. Romanoff and P. Varsta, "Bending response of web-core sandwich plates," *Composite Structures*, vol. 81, no. 2, pp. 292–302, 2007.

[5] K. Aghaee and M. Foroughi, "Mechanical properties of lightweight concrete partition with a core of textile waste," *Advances in Civil Engineering*, vol. 2013, Article ID 482310, 7 pages, 2013.

[6] H. Ousji, B. Belkassem, M. A. Louar, B. Reymen, L. Pyl, and J. Vantomme, "Experimental study of the effectiveness of sacrificial cladding using polymeric foams as crushable core

with a simply supported steel beam," *Advances in Civil Engineering*, vol. 2016, Article ID 8301517, 13 pages, 2016.

[7] C. Borsellino, L. Calabrese, and A. Valenza, "Experimental and numerical evaluation of sandwich composite structures," *Composites Science and Technology*, vol. 64, no. 10–11, pp. 1709–1715, 2004.

[8] A. Russo and B. Zuccarello, "Experimental and numerical evaluation of the mechanical behaviour of GFRP sandwich panels," *Composite Structures*, vol. 81, no. 4, pp. 575–586, 2007.

[9] H. Fang, H. M. Sun, W. Q. Liu, L. Wang, Y. Bai, and D. Hui, "Mechanical performance of innovative GFRP-bamboo-wood sandwich beams: experimental and modelling investigation," *Composites Part B: Engineering*, vol. 79, pp. 182–196, 2015.

[10] T. Sharaf, W. Shawkat, and A. Fam, "Structural performance of sandwich wall panels with different foam core densities in one-way bending," *Journal of Composite Materials*, vol. 44, no. 19, pp. 2249–2263, 2010.

[11] A. A. Prakash, B. Mohan, A. Rajadurai, and A. Jaswin, "Low velocity impact behaviour of glass fabric/epoxy honeycomb core sandwich composites," *Science and Engineering of Composite Materials*, vol. 22, no. 5, pp. 525–538, 2015.

[12] C. A. Steeves and N. A. Fleck, "Collapse mechanisms of sandwich beams with composite faces and a foam core, loaded in three-point bending. Part I: analytical models and minimum weight design," *International Journal of Mechanical Sciences*, vol. 46, no. 4, pp. 561–583, 2004.

[13] C. A. Steeves and N. A. Fleck, "Collapse mechanisms of sandwich beams with composite faces and a foam core, loaded in three-point bending. Part II: experimental investigation and numerical modeling," *International Journal of Mechanical Sciences*, vol. 46, no. 4, pp. 585–608, 2004.

[14] T. Keller and J. de Castro, "System ductility and redundancy of FRP beam structures with ductile adhesive joints," *Composites Part B: Engineering*, vol. 36, no. 8, pp. 586–596, 2005.

[15] A. C. Manalo, T. Aravinthan, and W. Karunasena, "Flexural behaviour of glue-laminated fiber composite sandwich beams," *Composite Structures*, vol. 92, no. 11, pp. 2703–2711, 2010.

[16] E. M. Reis, *Characteristics of Innovative 3-D FRP Sandwich Panels*, North Carolina State University, NC, USA, 2005.

[17] E. M. Reis and S. H. Rizkalla, "Material characteristics of 3-D FRP sandwich panels," *Construction and Building Materials*, vol. 22, no. 6, pp. 1009–1018, 2008.

[18] K. Mehmet, G. Hakan, K. Nevin, and I. Jan, "Static behavior of three-dimensional integrated core sandwich composites subjected to three-point bending," *Journal of Reinforced Plastics and Composites*, vol. 32, no. 9, pp. 664–678, 2013.

[19] M. Dawood, E. Taylor, and S. Rizkalla, "Two-way bending behavior of 3-D GFRP sandwich panels with through-thickness fiber insertions," *Composite Structures*, vol. 92, no. 4, pp. 950–963, 2010.

[20] W. G. James, *Influence of Reinforcement Type on the Mechanical Behavior and Fire Response of Hybrid Composites and Sandwich Structures*, The State University of New jersey, State of New Jersey, NJ, USA, 2004.

[21] L. Wang, W. Q. Liu, H. Fang, and L. Wan, "Behavior of sandwich wall panels with GFRP face sheets and a foam-GFRP web core loaded under four-point bending," *Journal of Composite Materials*, vol. 49, no. 22, pp. 2765–2778, 2015.

[22] L. Wang, W. Q. Liu, L. Wan, H. Fang, and D. Hui, "Mechanical performance of foam-filled lattice composite panels in four-point bending: experimental investigation and analytical modeling," *Composites Part B: Engineering*, vol. 67, pp. 270–279, 2014.

[23] ASTM, *Standard Test Method for Tensile Properties of Polymer Matrix Composite Materials*, ASTM D3039/D3039M-17, ASTM, West Conshohocken, PA, USA, 2017.

[24] ASTM, *Standard Test Method for Short-Beam Strength of Polymer Matrix Composite Materials and their Laminates*, ASTM D2344/D2344-16, ASTM, West Conshohocken, PA, USA, 2016.

[25] ASTM, *Standard Test Method for Compressive Properties of Rigid Cellular Plastics*, ASTM D1621/D1621-16, ASTM, West Conshohocken, PA, USA, 2016.

[26] ASTM, *Standard Test Method for Shear Properties of Sandwich Cores Materials*, ASTM C273/C273-16, ASTM, West Conshohocken, PA, USA, 2016.

[27] Z. Y. Sun, Y. Yang, W. H. Qin, S. T. Ren, and G. Wu, "Experimental study on flexural behavior of concrete beams reinforced by steel-fiber reinforced polymer composite bars," *Journal of Reinforced Plastics and Composites*, vol. 31, no. 24, pp. 1737–1745, 2012.

[28] P. Feng, S. Cheng, Y. Bai, and L. P. Ye, "Mechanical behavior of concrete-filled square steel tube with FRP-confined concrete core subjected to axial compression," *Composite Structures*, vol. 123, pp. 312–324, 2015.

[29] T. Belytschko, J. I. Lin, and C. S. Tsay, "Explicit algorithms for the nonlinear dynamics of shells," *Computer Methods in Applied Mechanics and Engineering*, vol. 42, no. 2, pp. 225–251, 1984.

[30] F. K. Chang and K. Y. Chang, "Post-failure analysis of bolted composite joints in tension or shear-out mode failure," *Journal of Composite Materials*, vol. 21, no. 9, pp. 809–833, 1987.

[31] F. K. Chang and K. Y. Chang, "A progressive damage model for laminated composites containing stress concentrations," *Journal of Composite Materials*, vol. 21, no. 9, pp. 834–855, 1987.

[32] J. Y. Chen, H. Fang, W. Q. Liu et al., "Energy absorption of foam-filled multi-cell composite panels under quasi-static compression," *Composites Part B: Engineering*, vol. 153, pp. 295–305, 2018.

[33] H. Yin, G. Wen, Z. Liu, and Q. Qing, "Crashworthiness optimization design for foam-filled multi-cell thin-walled structures," *Thin-Walled Structures*, vol. 75, no. 1, pp. 8–17, 2014.

[34] Z. H. Zhang, S. T. Liu, and Z. L. Tang, "Crashworthiness investigation of kagome honeycomb sandwich cylindrical column under axial crushing loads," *Thin-Walled Structures*, vol. 48, no. 1, pp. 9–18, 2010.

[35] S. P. Santosa, T. Wierzbicki, A. G. Hanssen, and M. Langseth, "Experimental and numerical studies of foam-filled sections," *International Journal of Impact Engineering*, vol. 24, no. 5, pp. 509–534, 2000.